



Air humidity characteristics of local climate zones: A three-year observational study in Nanjing



Xiaoshan Yang^a, Lilliana L.H. Peng^{a,*}, Yuan Chen^a, Lingye Yao^{a,b}, Qingqing Wang^a

^a Laboratory of Green Building and Eco-city, School of Architecture, Nanjing Tech University, Nanjing, 211816, China

^b State Key Laboratory of Subtropical Building Science, South China University of Technology, Guangzhou, 510641, China

ARTICLE INFO

Keywords:

Local climate zone
Urban humidity effects
Urban heat island
Atmospheric moisture
Urban meteorological network

ABSTRACT

Atmospheric humidity in the urban canopy layer is relevant to various fields, such as bioclimatology and public health. However, considerably less research has been conducted about urban effects on humidity than on temperature. This study aims to elucidate the spatiotemporal characteristics of humidity at the neighborhood scale. The humidity differences of 8 local climate zones (LCZs) in Nanjing, China, were analyzed based on three-year hourly observations. LCZ D (low plants) was used as the reference site. Differences in temperature (ΔT_{X-D}), relative humidity (ΔRH_{X-D}), and humidity ratio (ΔW_{X-D}) were investigated. The relationships of ΔW with condensation (dew and frost) and precipitation events, meteorological parameters, and ΔT were examined. The results show that variations in ΔRH_{X-D} exhibited a close inverse relationship with variations in ΔT_{X-D} . Greater negative ΔRH_{X-D} occurred during the nighttime when strong heat islands were present. Meanwhile, diurnal and seasonal patterns of ΔW_{X-D} were clearly observed. Greater and more frequent negative ΔW_{X-D} (moisture deficit) were observed during the daytime than during the nighttime and in warm months than in cold months, whereas the opposite trend was observed for positive ΔW_{X-D} (moisture excess). The frequency of urban moisture excess increased during the nighttime with heavy condensation. Precipitation events significantly increased the frequency of urban moisture excess, and this effect could last until 24 h after precipitation. ΔW was influenced by meteorological parameters, but the trends were not clear. No relation was observed between ΔW and ΔT . The findings can improve understanding of urban humidity and provide valuable information for humidity-related studies.

1. Introduction

Urbanization and human activities have modified climate in urban areas. Substantial studies have been conducted on the characteristics and causes of urban climates by focusing on temperature, airflow, radiation, and air pollution, among others. Atmospheric humidity in the urban canopy layer (UCL) has received less attention than other climatic elements in urban areas. However, existing studies have shown that UCL humidity considerably affects public health [1–3], urban air pollution [4,5], electric power consumption [6], human thermal comfort [7,8], and urban ecological system [9,10]. Considering the key roles of atmospheric humidity, the spatial and temporal characteristics of UCL humidity should be elucidated.

Two characteristics of atmospheric humidity were commonly discussed in the literature: relative humidity (RH) and actual water vapor content. Relative humidity, one of the most widely used measure, is a

function of temperature and water vapor content in air. Relative humidity is highly controlled by temperature, and patterns of relative humidity typically exhibit a close inverse relationship with temperature. Different measures have been used to determine the actual water vapor content in air: vapor pressure (hPa), dew point temperature (°C), absolute humidity (g/m³), specific humidity (g water/kg moist air), and humidity ratio (g water/kg dry air). Urban effects on UCL humidity are practically complex and dependent on a range of factors: synoptic conditions, urban morphology, urban thermal fields, relative lack of vegetation and extensive impervious surfaces, urban water bodies (lakes, rivers, ponds, fountains), advection, vertical turbulent transfer, anthropogenic sources of water vapor in the city (industries, combustion, cooling towers, etc.), and some particular weather events (precipitation, dew, frost, snowmelt, etc.) [11].

The present study aims to elucidate the spatiotemporal characteristics of atmospheric humidity at the neighborhood scale. Fixed-point

* Corresponding author. Add: NO.30 Puzhu Road (S), Nanjing, 211816, China.

E-mail address: plhblue@njtech.edu.cn (L.L.H. Peng).

measurement was employed to simultaneously collect air temperature and relative humidity from 8 local climate zones (LCZs) [12] across Nanjing for three years. Meteorological data were acquired from three national meteorological stations located in the suburban areas. In addition, morning condensation (dew and frost) in the suburb of Nanjing was recorded daily for one year. On the basis of these data, the characteristics of the relative humidity and humidity ratio of the LCZs were analyzed on multiple time scales (hourly, daily, monthly, and annual). The relationships of humidity ratio differences with condensation and precipitation events, meteorological parameters, and temperature differences were also examined.

2. Literature review

Oke et al. [11] have indicated that studies on UCL humidity are less complete than research on the urban heat island (UHI) and reports on UCL humidity are insufficient to establish comprehensive general principles. We conducted an extensive search on relevant studies published in peer-reviewed journals by focusing on the investigations of the canopy layer urban–rural humidity differences based on field observations. Ultimately, 27 case studies were included (Table 1).

On the basis of these studies (Table 1), some comments regarding the investigated topic are presented below:

- Most studies were conducted in the mid-latitude regions of Europe, North America, and Asia, particularly the cities with temperate climate (Köppen type C). Meanwhile, few studies were conducted in the tropical and arid cities. Relatively more studies were conducted in small- and medium-size cities. Therefore, conducting more studies in larger cities with varying climates is encouraged.
- The most widely used data to study urban effects on humidity were those from long-term fixed-station observations in urban and rural areas. Continuous data from urban and rural stations are indispensable in understanding the long-term temporal variance patterns of humidity under all weather conditions. However, most of the data collected were from a limited number of sites (usually one pair of urban–rural stations), suggesting the inadequacy of studies on the intra-city variabilities of humidity. Generally, the locations of those stations were originally selected not for studying urban influences but for other purposes, such as aviation or regional meteorology. Thus, the spatial representation of the stations may be insufficient for the study of local urban climates. A standard climate-based classification at local scale, such as the LCZ scheme [12] and the concept of urban tissue categories [41], can be used to select proper locations. Moreover, the use of a similar framework for site selection is particularly crucial to improve the comparability of studies and consequently more accurately quantify and comprehend urban effects on humidity.
- Mobile surveys were generally conducted for selected days under fine weather conditions. Data collected from mobile traverses can be used to generate humidity maps, which can be used to identify the spatial characteristics of humidity. Few studies have combined fixed-point measurements and mobile traverses. Moreover, most studies focused on urban–rural humidity differences, rarely discussing the effect of local surroundings on humidity.
- Mean RH values are often smaller in urban areas than in nearby rural areas. RH is highly controlled by temperature; thus, patterns of urban–rural RH differences usually exhibit a close inverse relationship with the patterns of urban–rural temperature differences. For instance, urban–rural RH differences tend to be greater during the nighttime and in certain seasons (may vary for different cities) when heat islands are stronger.
- The results reported in the literature are complex and diverse with respect to urban effects on atmospheric vapor content. Numerous studies have revealed that compared with air in nearby rural areas, urban air tends to exhibit more moisture during the nighttime and in

cold months but are drier during the daytime and in warm months. However, other patterns have also been reported, which have been attributed to various reasons. In addition, comparability of studies has to be improved with respect to site selection, measurement methods and periods, indicators, and classification of weather conditions.

3. Data and methods

3.1. Study area

Located in the Yangtze River Delta, the city of Nanjing (32°N, 118°E) is the capital of Jiangsu Province. In 2018, the city had an urban population of 6.96 million, according to the local government bulletin. Nanjing is characterized by hot summers and cold winters. Its climate is classified by the Köppen-Geiger system as Cfa (C: warm temperate; f: fully humid; a: hot summer) [40]. The Chinese Standard Weather Data [42] show the following climatic features: Nanjing had an average temperature of 2.2 °C during the coldest month (January) and 28.6 °C during the hottest month (July); the annual average wind speed was 2.2 m/s; during the period of October to March, the prevailing winds blew from the north (43%); during the period of April to September, the prevailing winds blew from the southeast (24%) and the south (22%); rainfall averaged 1106 mm annually, occurred mainly in summer.

An overview of the study area is presented in Fig. 1. Built-up areas and surrounding farmlands lie in the plains, with elevations ranging from 7 m to 30 m. The farmlands had been divided into small plots operated by individual households of nearby villages. The cultivated crops were quite diverse, generally without large-scale irrigation activities. Low mountains (elevation < 450 m), represented by large green areas in Fig. 1, are mainly covered with deciduous trees. The Yangtze River runs southwest–northeast through the city. Several lakes are found in the city, with the largest measuring about 3.7 km². Most residential buildings and small office buildings in Nanjing use split-type air conditioners for summer cooling, and large public buildings commonly use central air conditioning systems with cooling towers. Nanjing does not belong to the central heating area of China. Various types of distributed building heating solutions are used, including reversible split-type air conditioners, electric heaters, and gas boilers. The primary cooking energy source is natural gas. The number of registered vehicles in Nanjing was 2.74 million in 2018. There are no heavy industries in the main urban area of Nanjing.

3.2. Data

Field measurement in Nanjing started in July 2016 and is ongoing. As shown in Fig. 1, 14 sites distributed from the central districts to the peripheral areas were selected to monitor air temperature and relative humidity. Complete metadata and photographs of the 14 sites, as well as a detailed description of the field measurement, were given in Ref. [43]. The sites were selected based on the LCZ scheme, a standardized classification protocol for urban temperature studies [12]. LCZ is defined as an area with a minimum radius of 200–500 m, characterized by landscapes that are reasonably uniform in morphology, surface cover, land function, and human activity. Urban and rural landscapes are classified by the LCZ system into 17 LCZ types. An increasing number of studies have been conducted using the LCZ scheme for urban climate research. The literature (e.g. Ref. [44–47]), including our previous study on the thermal behavior of 14 LCZ sites [43], showed the good climatological relevance of the temperature regimes of LCZ classes to local surroundings.

In the present study, we selected 8 sites from the 14 LCZ sites for humidity analysis, namely: LCZs 2, 4, 5, 8, 10, A, G and D (Fig. 1). The sites included subclasses (LCZs 2₄, 2₃, 2_B, 5₆, 9₅, and B_E) were excluded. The purpose of selecting 8 standard LCZ classes is to better differentiate and display the humidity characteristics of different LCZ classes and to

Table 1

Summary of the canopy layer urban–rural humidity differences reported in 27 surveyed studies.

Year	City, latitude, climate, population ^a	Data description	Studied variables ^b	Main findings on urban–rural humidity differences	Refs.
1967	Leicester, 52°N, Cfb, 270 000	Car traverses, nights of Aug.	RH, VP	Nighttime RH: urban < rural. Nighttime VP was frequently higher in cities than in the nearby country.	[13]
1973	Chapel Hill, 35°N, Cfa, 29 000	Car traverses, Sep. and Oct.	DP	DP in the city was higher at night and lower in the morning and afternoon than DP in suburban and rural areas.	[14]
1975	Edmonton, 53°N, Dfb, 460 000	2 fixed stations, 13 years	RH, AH	In warm months, urban AH was lower by day but higher at night than rural AH. Urban snowmelt and rural dewfall significantly affect ΔAH.	[15]
1978	St. Louis, 38°N, Cfa	Multi-sources, Jul.	SH	SH was 10–20% less over the city than over upwind, rural areas.	[16]
1984	Shanghai, 31°N, Cfa	11 fixed stations, 30 years	RH, AH	For AH, urban moisture (dry) island occurs at night (day). ΔAH (city dry) was higher during a warm season than during a cold season.	[17]
1985	Lawrence, 38°N, Cfa, 48 000	Car traverses, summer and fall	DP	Surface materials and land use were correlated with morning and afternoon DPs but showed no significant correlation with evening DP.	[18]
1986	Phoenix, 33°N, BWh	1 fixed station, 1896–1984	RH, DP	DP was generally unchanged over the period; RH dropped sharply in recent decades.	[19]
1987	Chicago, 41°N, Dfa	2 fixed stations, 7 years	RH, VP, DP	Average urban–rural differences in vapor content were positive at night and negative in the forenoon and summer afternoons.	[20]
1987	Ibadan, 7°N, Aw, 2 million	3 fixed stations, 20 years	RH	The average urban–rural RH differences were about –3% at 09:00, and this difference increased to about –10% at 15:00.	[21]
1991	London, 51°N, Cfb	2 fixed stations, 10 years	VP	Urban areas were more humid than rural areas at night in all months and during the day in winter and spring but less humid in summer. ΔVP and UHI were well related.	[22]
1991	Ibadan, 7°N, Aw, over 2 million	3 fixed stations, 2 years	RH, VP	During daytime, both RH and VP were lower in the city than in the rural area.	[23]
1997	Mexico City, 19°N, Cwb	4 fixed stations, 1 year	SH	Urban air was more humid than rural areas at night, but this trend was reversed in the afternoon.	[24]
1999	Göteborg, 57°N, Cfb, 700 000	2 fixed stations, 4 years	VP	Urban–rural differences in humidity exert a significant influence on the energy balance in UHI.	[25]
1999	Szeged, 46°N, Cfb, 180 000	2 fixed stations, 3 years	VP	The city center was more humid than the rural area both by day and at night throughout the year.	[26]
2000	Pune, 18°N, BSh, 1.5 million	Car traverses, a night of Apr.	VP	At night, the city core appeared as moisture islands and at sunrise as dry islands.	[27]
2001	Belgrade, 44°N, Cfa, 1.2 million	4 fixed stations, 5 years	RH, VP	At 07:00 and 21:00, the urban area was more humid (Sep.–Feb.) but at 14:00 was drier for a full year. ΔVP and UHI were well associated.	[28]
2003	München, 48°N, Cfb	Fixed + mobile, summer + winter	VP	From the downtown to the suburban areas, mean VP decreased in summer but showed no significant variation in winter.	[29]
2005	Vancouver, 49°N, Csb	Fixed + mobile, summer	AH	Urban moisture excess observed on fine nights was linked to reduced urban dew. On grass, rural dewfall was greater than urban dewfall.	[30]
2006	Lódz, 51°N, Dfb, 800 000	2 fixed stations, 6 years	RH, VP	Urban–rural differences in VP could be positive or negative. The type of VP contrast that would occur was difficult to predict.	[31]
2007	Seoul and Busan, 37 & 35°N, Dwa & Cwa	5 fixed stations, 1905–2003	RH	Long-term change in RH in Seoul is dominated by a decreasing trend. The urban effect tends to be linked to city development.	[32]
2007	Krefeld, 51°N, Cfb, 238 000	2 fixed stations, 1 year	VP	Compared to the rural area, the urban area was more humid in 31.4% of the cases and rarely intense.	[33]
2009	Beijing, 39°N, Dwa, 17.4 million	2 fixed stations, 1971–2003	RH, VP	The urban area has lower VPs than the rural area at 08:00, 14:00 and 20:00, except at 02:00. In winter, urban VP was higher than the rural area and lower in other seasons.	[34]
2013	Ouagadougou, 12°N, BSh, 1.3 million	10 fixed stations, dry seasons	SH	At night, SH was higher at the vegetated site than at the sparsely vegetated urban center.	[35]
2018	Belgrade, 44°N, Cfa	2 fixed stations, 27 years	RH, VP	Monthly RH and VP were greater at the rural than urban station.	[36]
2018	São José do Rio Preto, 20°S, Aw	9 fixed stations, Jun. and Jul.	AH	Built environment configurations significantly influence the distribution of humidity through urban spaces.	[37]
2018	Beijing, 39°N, Dwa, 21.5 million	4 fixed stations, 2005–2014	RH	Population movement out of the city during the Chinese New Year holiday could increase urban RH relative to the non-holiday period.	[38]
2019	Yangtze River Delta urban agglomeration, 28–34°N, Cfa	145 fixed stations, 1961–2014	RH, VP, SH	Urban dry island effect (RH, VP, SH) was significantly intensified by urban expansion. These effects were particularly strong in wet hot summer and relatively weak in cold dry winter.	[39]

^a The climate types of the cities are in accordance with the Köppen-Geiger climate classification [40]. Population data are included if reported in the reference.^b RH: relative humidity, %; VP: vapor pressure, hPa; DP: dew point temperature, °C; AH: absolute humidity, g/m³; SH: specific humidity, g/kg.

improve comparability with other studies. The classifications, satellite images, and properties of the 8 LCZ sites are listed in [Table 2](#). Hourly air temperature and relative humidity for each LCZ site were collected from three points located in the core area of each site within a radius of 100 m. The yellow dots in the satellite images ([Table 2](#)) show the locations of the monitoring points. For LCZs 10, A, and D, two monitoring points were mounted due to the lack of proper lampposts or poles. For LCZ G (water), three monitoring points were mounted but two of them are situated on the banks of the islands in the lake. The two points may not sufficiently represent LCZ G (water) because a considerable proportion of their thermal source area is land. Therefore, we only used the point

situated on the long and narrow walkway cross the lake (see the satellite image of LCZ G in [Table 2](#)) for analysis. About 90% of the area around the point (a radius of 200 m) is water. [Fig. 2](#) shows the data logger used and its installation.

Sources of the data used in the present study are listed in [Table 3](#):

- (1) Hourly air temperature and relative humidity were collected from the fixed points of each site (as shown in [Table 2](#)). At each point, a temp/RH data logger (HOBO U23-001 Pro v2) housed inside a matching radiation shield was mounted on lampposts or poles at 2.3–2.7 m above ground ([Fig. 2](#)). The data logger has an

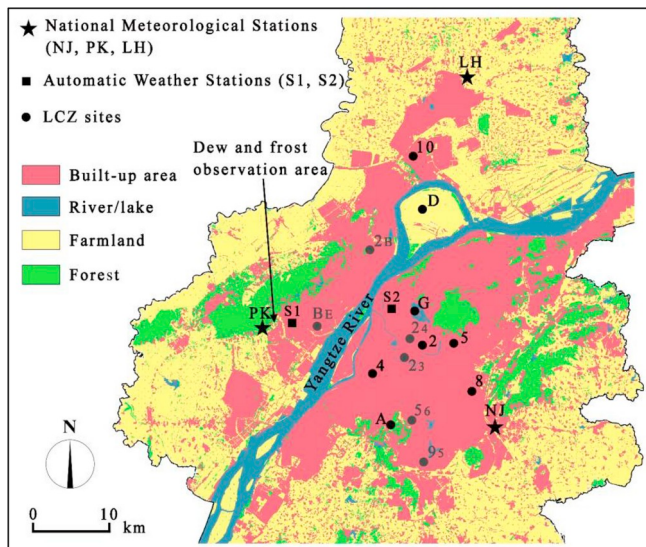


Fig. 1. Overview of the study area, local climate zone (LCZ) sites, and weather stations (modified after [43]). The character(s) attached to each LCZ site represents its LCZ type. The LCZ sites marked with black dots were analyzed in this study.

uncertainty of ± 0.21 °C from 0 to 50 °C and $\pm 2.5\%$ from 10% to 90% RH, with a resolution of 0.02 °C/0.05% RH. The stability (drift per year) of the data logger is less than 0.1 °C/1% RH. The site temperature and humidity were calculated using the average measurements of the points.

- (2) Hourly meteorological data were gathered from three suburban national meteorological stations (NMSs) and two automatic weather stations (AWSs) we built (Fig. 1). The NMSs are standard ground stations, which form part of the World Meteorological Organization networks. The hourly data of the NMSs, including air temperature, relative humidity, wind speed, wind direction, atmospheric pressure, and precipitation, can be accessed via China Meteorological Data Service Center (CMDC). However, solar radiation and cloud cover are not available in the CMDC data products. In this study, global horizontal solar radiation was measured from the two AWSs mounted on the rooftops. No consistent statistically significant difference in solar radiation intensity was found between the two AWSs, and the mean values were used. The amount of hourly cloud over the study area was extracted from the FY2G satellite data available in the CMDC.
- (3) We also conducted observations on daily condensation events (dew and frost) for one year (August 1, 2018–July 31, 2019). Daily condensation was manually recorded by taking photographs of the open grasslands in the peripheral area of the city (Fig. 1) because of the lack of instruments to measure dewfall (e.g. mini-lysimeters). The surveyed grasslands were left unmaintained and were not irrigated during the observational period. The records represent suburban dewfall on grassland because of its location. In this study, we did not record the condensation in urban areas. The daily observation campaigns were conducted between 05:00 a.m. and 08:00 a.m. A total of 87 days had no observations recorded because of schedule conflicts. In addition, to reduce the influence of precipitation events, the days when the nearby paved surface was wet when taking photographs were excluded. Ultimately, a total of 223 days with valid records were used. These 223 days were classified, by the extent of daily morning condensation, into three levels: heavy, light, and none.

3.3. Methods

Hourly measurements collected from the 8 LCZ sites and the meteorological stations for a three-year period (August 1, 2016–July 31, 2019) were used to analyze humidity. For simplification, the period from August 1, 2016 to July 31, 2017 is referred to as “2017” and the subsequent two years are referred to as “2018” and “2019”, respectively. Two measures of humidity were employed: relative humidity and humidity ratio (g water/kg dry air). The humidity ratio of each LCZ site was not directly measured but instead was calculated using the building energy simulation program EnergyPlus [48], with the values of the air temperature and relative humidity measured at the LCZ sites, and the values of the mean atmospheric pressure measured from the NMSs. The differences in relative humidity and humidity ratio between LCZ D and the other LCZ sites (LCZ X–LCZ D) were analyzed. LCZ D was selected as the reference site for two reasons: (i) LCZ D (low plants) represents a typical non-urbanized landscape and (ii) the same data logger used at the sites can reduce the systematic biases caused by different instruments. The farmland at LCZ D had been divided into small plots operated by individual households of the nearby village. During the three-year investigation, the crops at LCZ D were diverse and mixed (vegetable, plant nursery, wheat, etc.) and no extensive irrigation was observed. In the analysis below, differences in air temperature, relative humidity, and humidity ratio are expressed as ΔT_{X-D} , ΔRH_{X-D} , and ΔW_{X-D} , respectively. The subscript letter “X” denotes the LCZ site analyzed.

The average amounts of precipitation of the five weather stations (3 NMSs + 2 AWSs) were used. The days with daily accumulated precipitation ≥ 0.1 mm (the lower limit of light precipitation events) were identified as precipitation days. Over the three-year period, 10 days had snowfall. In Nanjing, snowfall was usually mixed with rainfall, and snow cover rarely remained for longer than a week. In the analysis, the 10 days with snowfall were treated as common precipitation days. The temporal patterns of urban–rural moisture differences seem to be best exhibited in “ideal” weather conditions (calm, clear), similar to the UHI [11]. In this study, the weather factor (Φ_W) proposed by Oke [49] was used to identify ideal days suitable for the development of local climates:

$$\Phi_W = u^{-1/2} (1 - kn^2) \quad (1)$$

where u is the regional wind speed (m/s), the coefficient k is associated with cloud types, and n is the fraction of cloud coverage [50]. Φ_W , which ranges from 0 to 1, measures the extent to which sky and wind conditions are suitable for UHI development. Wind speeds from the three NMSs were averaged to represent regional wind speed. The hourly weather factor was calculated using hourly wind and cloud data, and the daily averages were obtained. The criterion for selecting ideal days is the daily mean $\Phi_W \geq 0.7$ and without precipitation, which is consistent with previous studies [43,44,46]. Table 4 lists by month the number of precipitation days and ideal days for the three-year period.

The characteristics of ΔT_{X-D} shown in this study are similar to those described in our earlier report [43], which was based on a data set of 401 days collected from 14 LCZ sites. However, in the subsequent sections, the ΔT , ΔRH , and ΔW for the three-year period are presented because the characteristics of ΔRH and ΔW cannot be discussed independent of ΔT . In the current study, we mainly focus on the characteristics of ΔRH and ΔW . A detailed analysis of the characteristics of ΔT_{X-D} can be found in Ref. [43].

4. Results

4.1. Hourly differences

The differences in hourly temperature, relative humidity, and humidity ratio between LCZ 2 (compact mid-rise) and LCZ D (low plants) for 2019 were used to illustrate temporal patterns (Fig. 3). A clear

Table 2

Metadata for the 8 local climate zone (LCZ) sites in Nanjing (modified after [43]). Yellow dots represent Temp/RH monitoring points. Site metadata are the mean values of each site with a radius of 500 m.

Satellite image	Properties ^a	Satellite image	Properties ^a
	<p>LCZ 2: compact mid-rise – Site metadata: SVF: 0.41 Building: 34% * Impervious: 55% * Pervious: 11% Z_{H^*}: 16 m – Land function: residential, commercial</p>		<p>LCZ 10: heavy industry – Site metadata: SVF: 0.74 Building: 29% Impervious: 51% * Pervious: 20% * Z_{H^*}: 12 m – Land function: industrial (petrochemical plants)</p>
	<p>LCZ 4: open high-rise – Site metadata: SVF: 0.48 * Building: 14% * Impervious: 48% * Pervious: 38% Z_{H^*}: 36 m – Land function: residential</p>		<p>LCZ A: dense trees – Site metadata: SVF: Building: 1% Impervious: 2% Pervious: 97% Z_{H^*}: 8 m – Land function: forest (deciduous)</p>
	<p>LCZ 5: open mid-rise – Site metadata: SVF: 0.40 * Building: 20% Impervious: 44% Pervious: 36% Z_{H^*}: 17 m – Land function: institutional (campuses)</p>		<p>LCZ G: water – Site metadata: SVF: Building: 2% Impervious: 4% Pervious: 94% (water: 79%) Z_{H^*}: – Land function: recreational (urban lake)</p>
	<p>LCZ 8: large low-rise – Site metadata: SVF: 0.68 * Building: 34% Impervious: 42% Pervious: 24% * Z_{H^*}: 11 m * – Land function: commercial (auto sales & services)</p>		<p>Reference site LCZ D: low plants – Site metadata: SVF: 0.91 Building: 2% Impervious: 5% Pervious: 93% Z_{H^*}: <1 m – Land function: agriculture (vegetable, wheat)</p>

^a SVF = mean sky view factor at ground level (including trees); Building = building coverage; Impervious = impervious surface; Pervious = pervious surface; Z_h = geometric average of building or plant heights; ‘—’ indicates data is not available; ‘*’ indicates the value slightly lies outside the suggested range of the corresponding LCZ type given in Ref. [12].

pattern of the daily cycle of ΔT_{2-D} was observed, as reported in our earlier study [43]; UHI intensities were higher from sunset to about 2 h after sunrise and lower or even negative (cool islands) during the daytime (sunrise+2 h to sunset). The striated pattern throughout the year indicates that weather conditions played an important role in the formation of UHI. Variations in ΔRH were closely associated with variations in ΔT over the year. For most of the year, the RH values were lower at LCZ 2 than at LCZ D, with greater deficits occurring when strong heat islands were present. During the daytime (sunrise+2 h to sunset), $\Delta RH_{2-D} > 0$ occasionally occurred when cool islands were present.

Humidity ratio differences (ΔW_{2-D}) are more complex than differences in ΔRH and ΔT . ΔW could be positive or negative throughout the year. However, a less clear pattern was observed from the results; positive ΔW occurred more frequently during the nighttime and in cold months (December–February), whereas negative ΔW occurred more frequently during the daytime and in warm months (May–October). Compared with the relationship between ΔRH and ΔT , the visible linkage between ΔW and ΔT was less clear although existent. Relatively great moisture deficits ($\Delta W < 0$) usually occurred with strong UHI, particularly for continuous days with higher UHI intensities than usual. Given the different features of ΔT , ΔRH , and ΔW between the daytime (sunrise+2 h to sunset) and nighttime (sunset to sunrise+2 h), the concept of splitting a day into the two time spans was adopted in the following analysis.

4.2. Annual mean differences

Fig. 4 presents the distributions of the daily averages of ΔT_{X-D} , ΔRH_{X-D} , and ΔW_{X-D} during the nighttime and during the daytime for all days and ideal days. The RH differences among the LCZ sites were significant during the nighttime (Fig. 4c) but negligible during the daytime (Fig. 4d). For an LCZ site, the higher the heat island intensities, the lower the RH . The nighttime mean ΔRH_{X-D} values ranged from -1% to -9% under all weather conditions and from -2% to -13% under ideal weather conditions (Fig. 4c). Under all and ideal weather conditions, the daytime mean ΔRH_{X-D} values were relatively small, ranging from $+2\%$ to -5% (Fig. 4d). LCZ G is a large lake, where the nighttime mean RH values were lower than that of LCZ D.

The daily nighttime and daytime averages of humidity ratio differences (ΔW_{X-D}) for all days and ideal days are shown in Fig. 4e and f, respectively. The characteristics of ΔW_{X-D} varied from those of ΔRH_{X-D} .



Fig. 2. The temp/RH data logger used in this study and a monitoring point in the site LCZ 5.

First, all LCZ sites, except for LCZ A, showed greater moisture deficits (drier) during the daytime than during the nighttime. Second, the mean humidity ratio differences among the LCZ sites were not significant during the daytime and nighttime. Third, no clear relationship was found between ΔW_{X-D} and ΔT_{X-D} . For the majority of the LCZ sites, the mean moisture deficits were slightly greater under ideal weather conditions than under all weather conditions. Compared with LCZ D, LCZ G had a lower mean humidity ratio during the daytime and a higher humidity ratio during the nighttime under all weather conditions. Possible explanations for this are discussed in Section 5.2.

4.3. Seasonal variations

The monthly averages of air temperature, relative humidity, and humidity ratio at the reference site (LCZ D) are shown in Fig. 5 by year. No notable inter-annual variations occurred over the three years. The relative humidity values showed no seasonal variations, whereas the humidity ratios exhibited significant seasonal variations, with the maximum occurring in the summer and the minimum in the winter.

The monthly average differences in air temperature (ΔT_{X-D}), relative humidity (ΔRH_{X-D}), and humidity ratio (ΔW_{X-D}) for all days are shown in Fig. 6. For all LCZ sites, except for LCZ A, the monthly mean ΔRH_{X-D} values exhibited no seasonal patterns, similar to ΔT_{X-D} . As shown in Fig. 6c and d, LCZs 2, 4, 10, and G showed greater decreases in RH during the nighttime than during the daytime for all months, whereas LCZs 5 and 8 showed no significant night-day RH differences. In the warm months, the daytime RH values at LCZ A were slightly higher than those at LCZ D (Fig. 6d).

A clear seasonal pattern was observed from the monthly mean ΔW_{X-D} values (Fig. 6e and f). The differences in humidity ratio (ΔW_{X-D}) were greater in warm months than in cold months. During the daytime for a whole year, all LCZ sites generally contained less water vapor in the air relative to LCZ D, with greater deficits in warm months and smaller deficits in cold months (Fig. 6f). Meanwhile, the nighttime ΔW_{X-D} values tended to change from deficits ($\Delta W < 0$) in warm months to slight excesses ($\Delta W > 0$) in cold months (Fig. 6e). LCZ G exhibited more moisture than LCZ D ($\Delta W_{G-D} > 0$) during the nighttime for all months, except for July and August, but was drier ($\Delta W_{G-D} < 0$) during the daytime for all months.

The monthly average differences in ΔT_{X-D} , ΔRH_{X-D} , and ΔW_{X-D} for the ideal days are shown in Fig. 7. The seasonal patterns of ΔT_{X-D} , ΔRH_{X-D} , and ΔW_{X-D} under ideal weather conditions were generally similar to those under all weather conditions, except that the differences are greater.

Table 3
Description of the data used.

Variables ^a	Source	ID in Fig. 1	Description
Tair, RH (site-specific)	8 selected LCZ sites	2, 4, 5, 8, 10, A, G, D	Each site has 1–3 monitoring points, as specified in Table 2.
Tair, RH, WIN, PRS, PRE	3 national meteorological stations	NJ, PK, LH	Standard ground stations (as part of the World Meteorological Organization networks)
PRE, SW	2 automatic weather stations	S1, S2	Installed on rooftops by the authors
Daily morning dew & frost	Manually taking photos of open grasslands	The specified area	During the period 05:00 a.m.–08:00 a.m. from August 2018 to July 2019

^a Tair: air temperature; RH: relative humidity; WIN: wind speed and direction; PRS: atmospheric pressure; PRE: precipitation; SW: solar radiation.

Table 4Number of precipitation days and “ideal” days for the three-year period (August 1, 2016–July 31, 2019)^a.

Month	Jan	Feb	Mar	Apr	May	Jun	Jul	Aug	Sep	Oct	Nov	Dec	Total
Precipitation days (accumulated amount, mm)	36 (197)	34 (147)	33 (145)	34 (184)	36 (309)	24 (419)	38 (420)	48 (535)	39 (467)	42 (419)	34 (174)	31 (181)	429 (3595)
Ideal days	23	21	24	22	17	20	15	16	16	28	30	36	268

^a The definitions of “precipitation days” and “ideal” days are given in the text. The precipitation days include 10 days of snowfall mixed with rainfall.

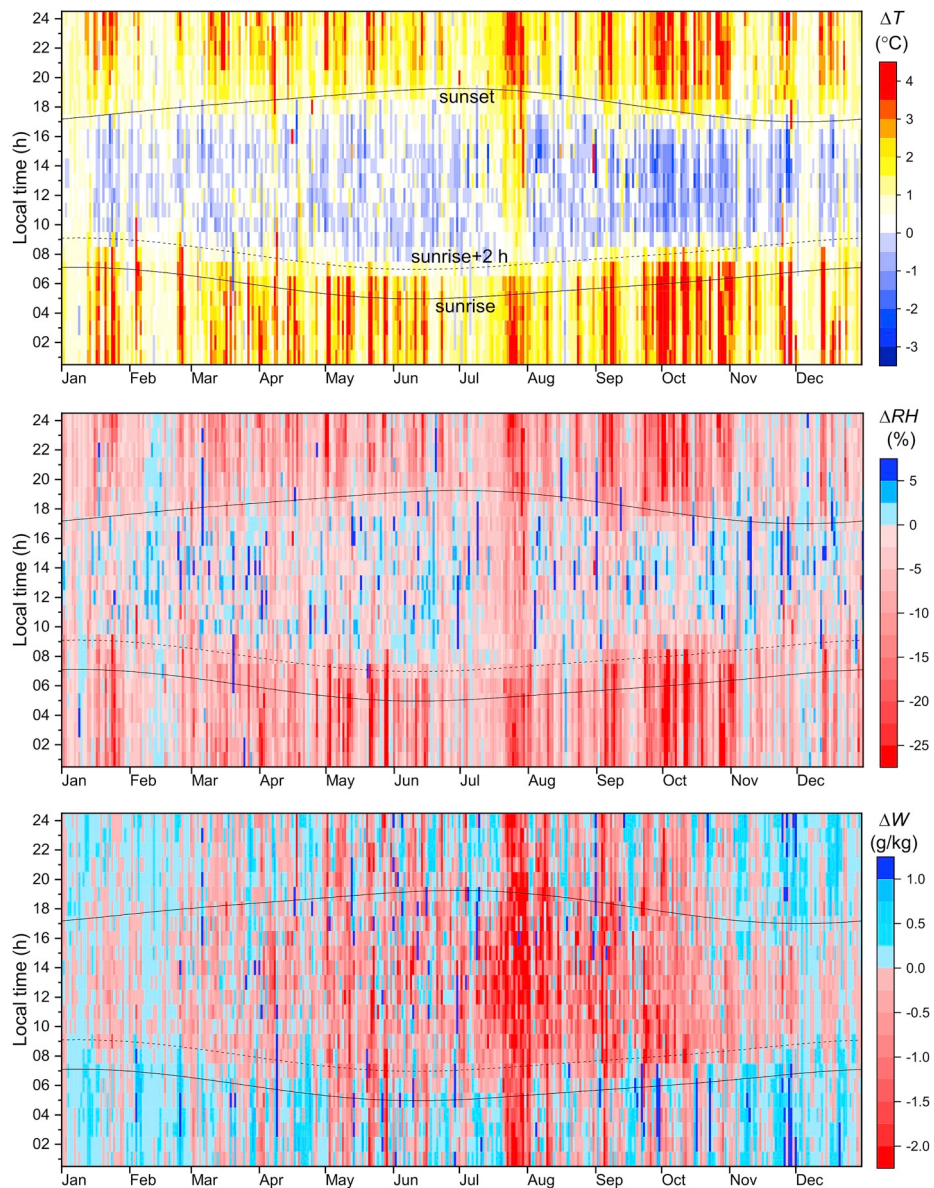


Fig. 3. Hourly differences (LCZ 2–LCZ D) in air temperature (ΔT), relative humidity (ΔRH), and humidity ratio (ΔW) for 2019.

4.4. Diurnal variations

Mean diurnal variations in ΔT_{X-D} , ΔRH_{X-D} , and ΔW_{X-D} were calculated by averaging the data for 23 ideal days in January and 15 ideal days in July over the three years. To clearly show the diurnal courses, we selected LCZs 2, A and G to depict the characteristics of the daily cycles (Fig. 8).

The curves of ΔRH_{X-D} generally show the inverse patterns of the ΔT_{X-D} curves. In both January and July, the RH differences among the LCZ sites narrowed quickly after sunrise and widened in the late afternoon and the evening (Fig. 8c and d). The RH values at the extensively

urbanized site (LCZ 2) were lower than those at LCZ D throughout the day, with a maximum difference of about –20% during the nighttime in July. Notably, the RH values at LCZ G were not higher than those at LCZ D throughout the day in both January and July and even around midday when weak cool islands occurred ($\Delta T_{G-D} < 0$). RH was lower at LCZ A than at LCZ D during the nighttime of January; however, RH was higher during the daytime in July.

Significant difference in ΔW_{X-D} between January and July was observed (Fig. 8e and f). The diurnal pattern of the humidity ratio at LCZ D (denoted by hollow dots in Fig. 8e and f) needs to be discussed before analyzing ΔW_{X-D} . First, the humidity ratio at LCZ D was considerably

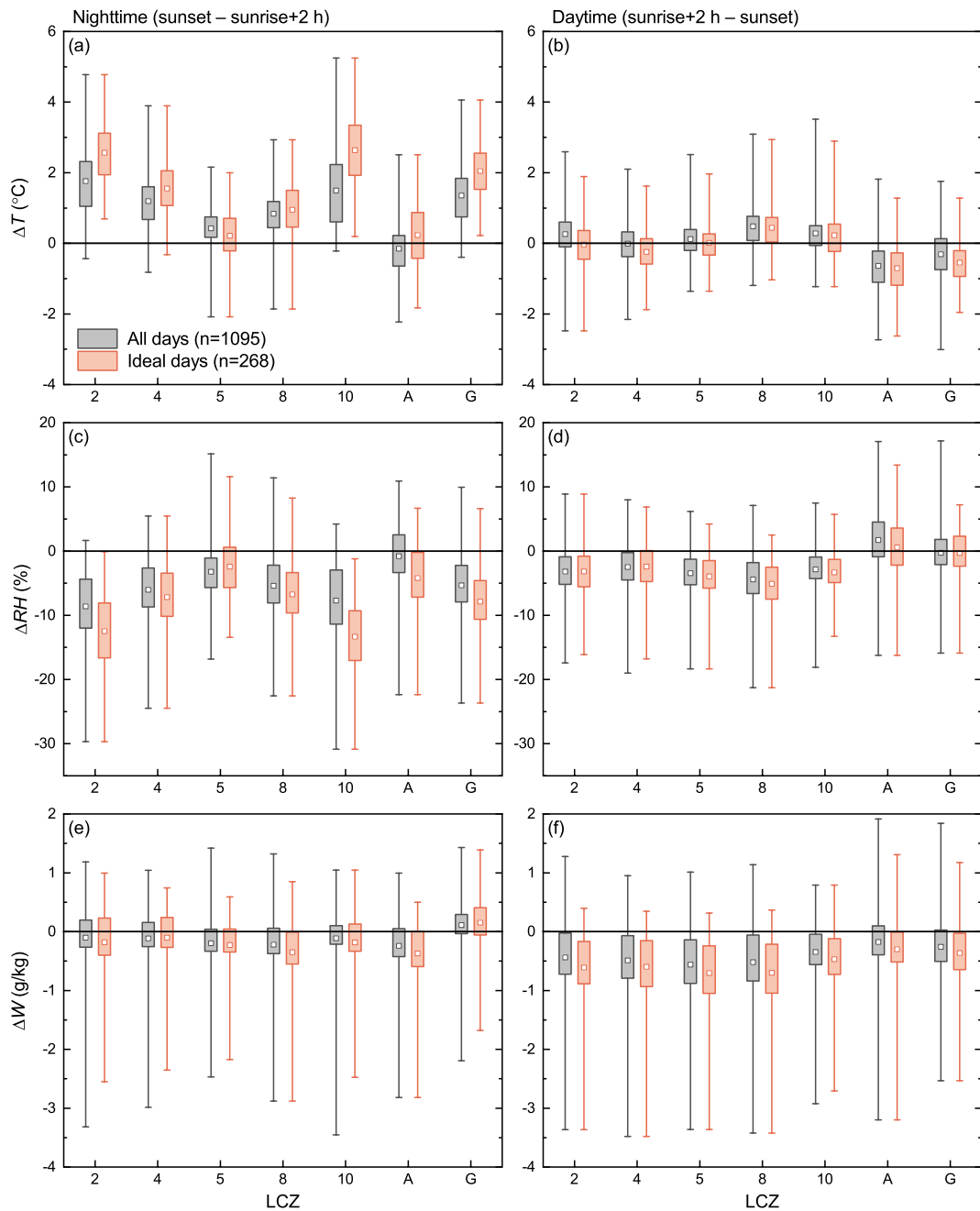


Fig. 4. Distributions of the nighttime (left) and daytime (right) average differences in air temperature (ΔT), relative humidity (ΔRH), and humidity ratio (ΔW) between the LCZ sites (LCZ X–LCZ D). Each box encompasses 50% of the data; the square is the mean, and the ends of vertical lines represent the maximum and minimum values.

higher in July than in January because of intense evapotranspiration in the summer. Second, LCZ D exhibited a peak in January (several hours after sunrise) and two peaks in July (one peak appeared several hours after sunrise and another peak appeared several hours after sunset). Observations on clear days in the summer from Edmonton [15] also showed a similar double peak, except that the second peak occurred just before sunset. Possible causes of this phenomenon were identified [11, 15]: the morning peak in moisture was probably due to the onset of evaporation into a shallow mixing layer capped by remnant nocturnal inversion; the second peak before or after sunset probably occurred because atmospheric stability increased around sunset but evaporation continued. No second peak occurred in January could be related to the intensity of evaporation being small around sunset in cold winter.

In January, the ΔW_{X-D} values were small (within ± 0.5 g/kg),

tending to be negative by day but near zero or positive values during the nighttime (Fig. 8e). Compared with those in January, the ΔW_{X-D} values in July were considerably greater with intense fluctuations during the daytime (Fig. 8f). The LCZ sites in July generally showed moisture deficits ($\Delta W_{X-D} < 0$) throughout the day, with greater deficits occurring during the daytime. During the daytime in July, LCZ 2 was the driest site, whereas LCZ A showed the least deficits. Notably, the humidity ratio at LCZ G was apparently lower (drier) than at LCZ D during the daytime.

4.5. Frequency statistics

The nighttime and daytime frequencies of ΔRH_{X-D} types for the three years are shown in Fig. 9. For LCZs 2, 4, 5, 8 and 10, $\Delta RH_{X-D} <$

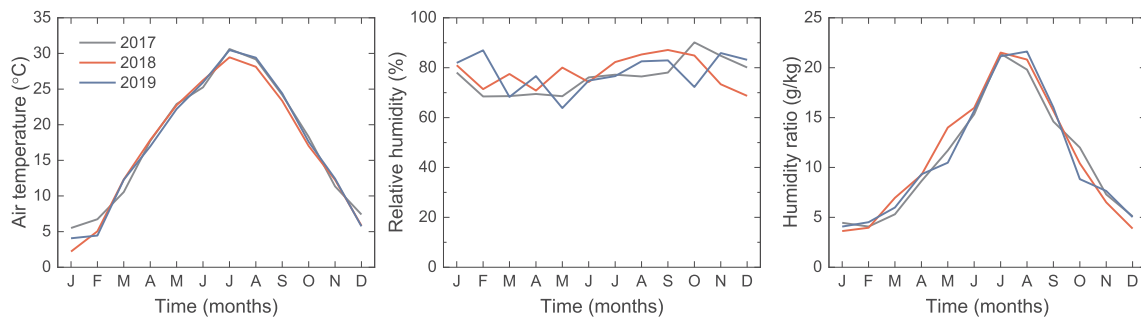


Fig. 5. Monthly averages of air temperature, relative humidity, and humidity ratio at the reference site (LCZ D) for the three years.

0 was clearly the dominant type both during the daytime and nighttime. The RH values at LCZ 2 were lower than those at LCZ D for more than 90% of the nighttime. The RH values at LCZ G were lower than those at LCZ D for more than 80% of the nighttime. At LCZ A, $\Delta RH_{A-D} > 0$ occurred more frequently, particularly during the daytime. For all LCZ sites, except for LCZ 5, $\Delta RH_{X-D} < 0$ occurred more frequently during the nighttime than during the daytime.

Notable differences in humidity ratio (ΔW_{X-D}) between night and day and between warm and cold season are described in Section 4.3. Therefore, we calculated the nighttime and daytime frequencies of ΔW_{X-D} types for the colder months (October–March) and the warmer months (April–September) (Fig. 10). The results showed a clear temporal characteristics: the frequency of $\Delta W_{X-D} > 0$ was higher during the nighttime than during the daytime, as well as in the cold months than in

the warm months. The LCZ sites exhibited more moisture than LCZ D for more than half of the nighttime in the cold months. No clear trend was observed for differences in the frequency of ΔW_{X-D} types among the LCZ sites.

4.6. Relationship between ΔW and particular weather events

In the current study, the suburban condensation events (dew and frost) observed over 223 days were classified into three levels: heavy, light, and none. The frequencies of the ΔW_{2-D} types among different levels of condensation events during the 01:00 a.m.–06:00 a.m. period were compared, as shown in Fig. 11. The 01:00 a.m.–06:00 a.m. interval was chosen because condensation events were generally most pronounced during the period. Relative to the results collected for all 223

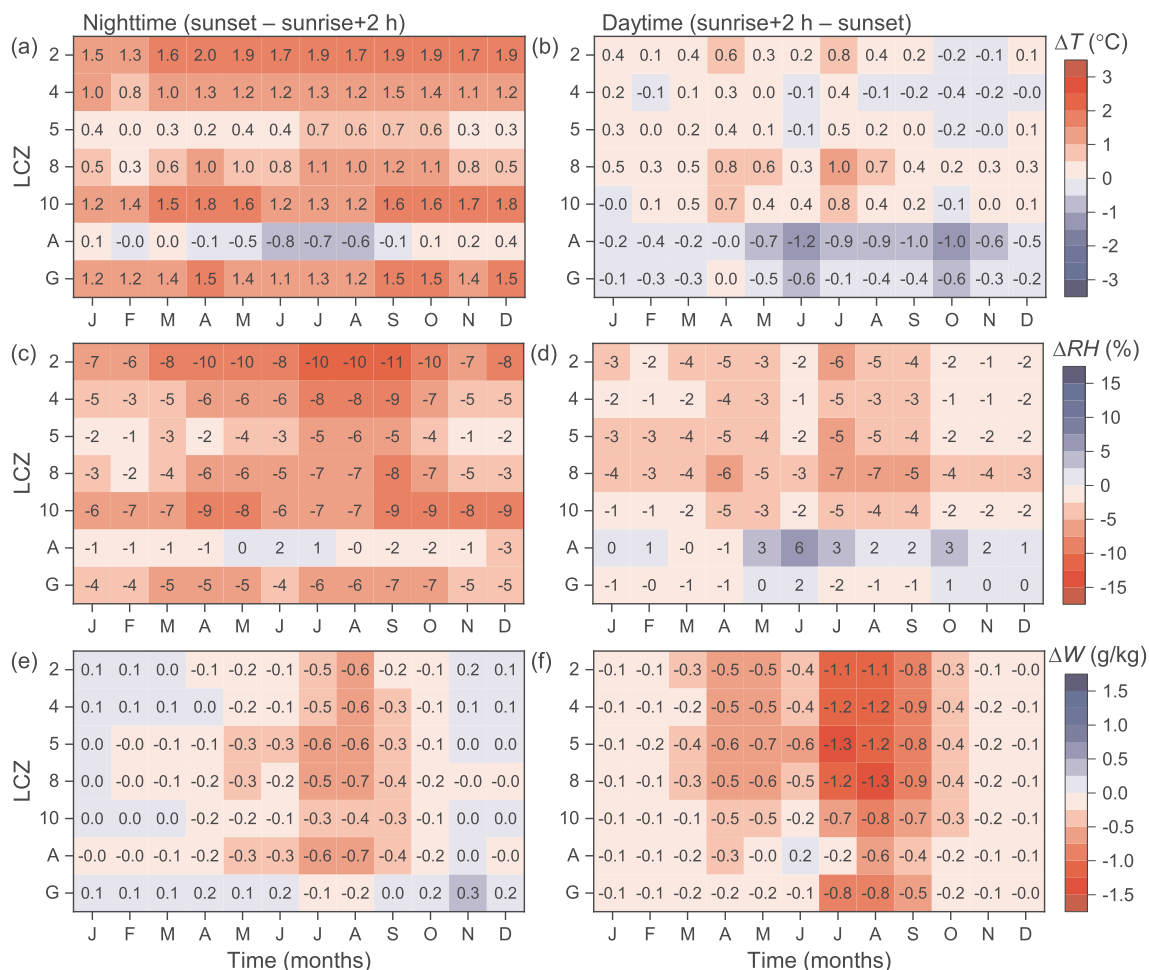


Fig. 6. Monthly mean differences in air temperature (ΔT_{X-D}), relative humidity (ΔRH_{X-D}), and humidity ratio (ΔW_{X-D}) for all days (n = 1095). On the left are the nighttime (sunset – sunrise+2 h) averages, and on the right are the daytime (sunrise+2 h – sunset) averages.

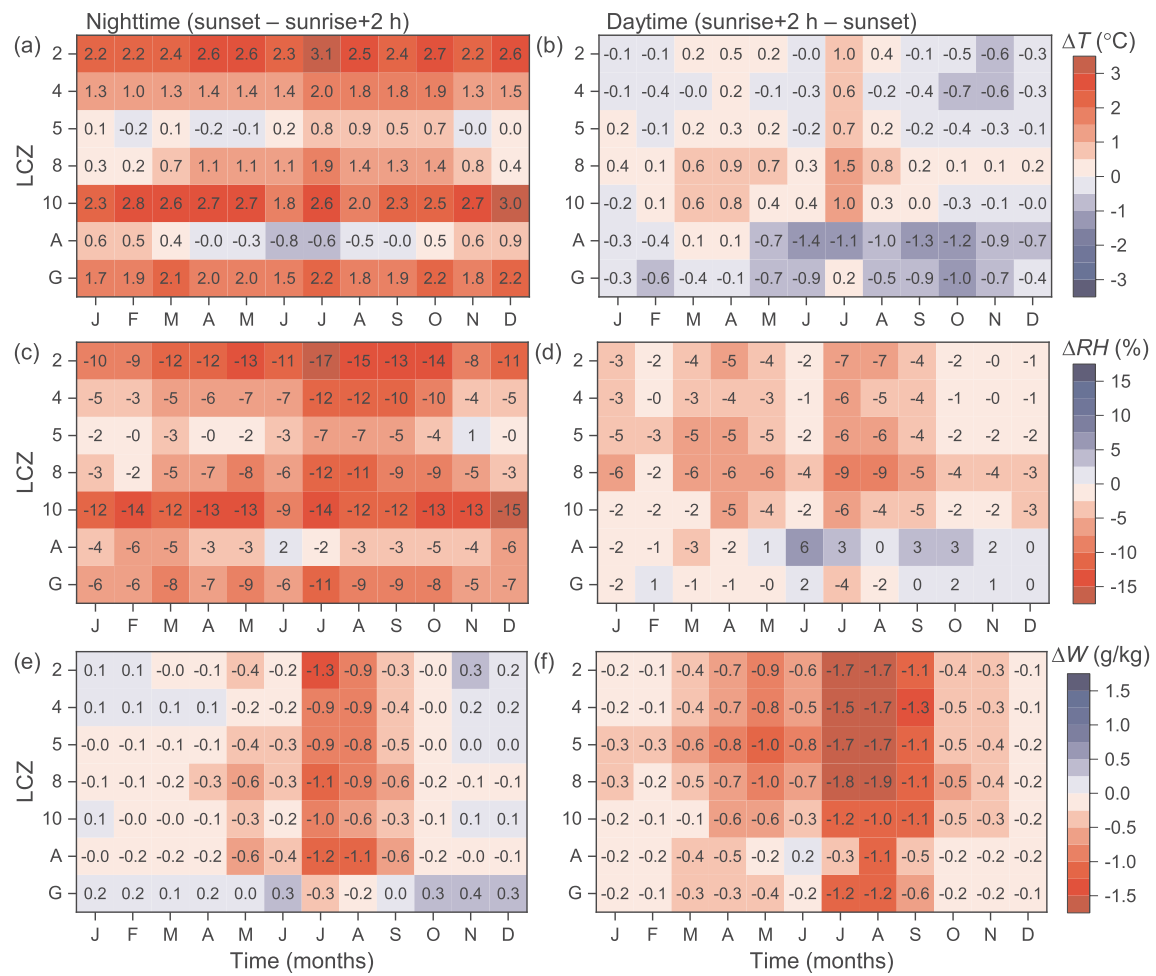


Fig. 7. Monthly mean differences in air temperature (ΔT_{X-D}), relative humidity (ΔRH_{X-D}), and humidity ratio (ΔW_{X-D}) for ideal days ($n = 268$). On the left are the nighttime (sunset – sunrise+2 h) averages, and on the right are the daytime (sunrise+2 h – sunset) averages.

days, the frequency of $\Delta W_{2-D} > 0$ was increased by 5% on days with heavy condensation; however, it decreased by 2% on days with light condensation and by 8% on days without condensation.

The effect of precipitation events on the frequency of ΔW_{2-D} types was also evaluated. The frequencies of hourly ΔW_{2-D} types were calculated for the following periods: the whole three years, during precipitation events, within 24 h after precipitation events, and within 25–48 h after precipitation events (Fig. 12). Bias could be caused by non-simultaneous precipitation in the study area; thus, only the hours when all five weather stations (3 NMSs + 2 AWSs) showed precipitation were considered as frequencies during precipitation events. Compared with the whole three-year period, the frequency of $\Delta W_{2-D} > 0$ increased by more than two times during the precipitation events (from 43% to 88%) and by 21% for the period within 24 h after the precipitation events. However, for the period within 25–48 h after the precipitation events, the frequency of $\Delta W_{2-D} > 0$ was slightly lower than that for the whole period.

4.7. Relationship between ΔW and meteorological variables

In this section, LCZ 2 is used as an example to illustrate the relationships between the daily average differences in humidity ratio (ΔW_{2-D}) and the daily averages of meteorological parameters, including cloud cover, global horizontal solar irradiance, suburban wind speed, and suburban relative humidity (Fig. 13). The days with precipitation were excluded from the three-year period, leaving 664 days for analysis. The humidity ratio differences (ΔW_{2-D}) were reduced with an increase

in cloud cover (Fig. 13a). Greater negative ΔW_{2-D} values were observed on the days with low values for cloud cover—specifically, less than 10% in this study. Moisture deficits (negative ΔW_{2-D}) generally increased with increasing solar irradiance (Fig. 13b). The relationship between ΔW_{2-D} and regional wind speed was unclear (Fig. 13c). Greater differences in humidity ratio occurred under relatively low wind speed conditions. ΔW_{2-D} and regional relative humidity were roughly correlated (Fig. 13d). Frequently moderate moisture deficits ($\Delta W_{2-D} < 0$) and rare moisture excess ($\Delta W_{2-D} > 0$) were generally observed when the suburban daily mean RH was less than 50%. A wide range of ΔW_{2-D} values, including great moisture deficits, was observed when the suburban daily mean RH was within 50%–80%. ΔW_{2-D} switched from moisture deficit to excess when the suburban daily mean RH exceeded 80%.

4.8. Relationship between ΔW and ΔT

Using the data of the 664 days without precipitation, we examined the relationships between the daily averages of ΔW_{2-D} and ΔT_{2-D} (averaged for nighttime and daytime, respectively). During the nighttime, a wider range of ΔW_{2-D} values was observed when heat island intensity increased, but no clear relationship was established between ΔW_{2-D} and ΔT_{2-D} (Fig. 14a). During the daytime, ΔW_{2-D} and ΔT_{2-D} seemed negatively correlated (Fig. 14b). Overall, no clear relationship was found between humidity ratio differences and heat island intensities in this study.

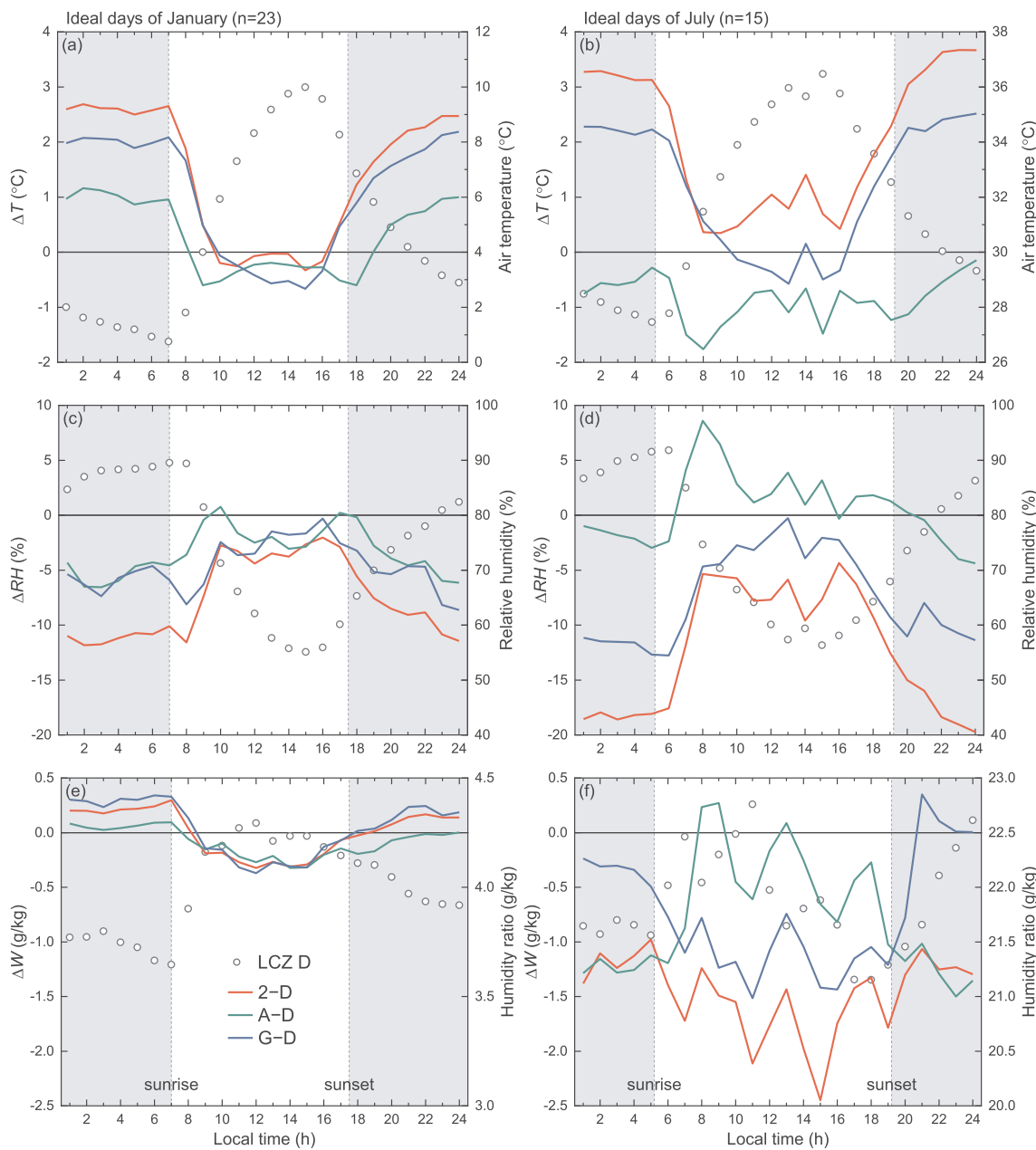


Fig. 8. Mean diurnal variations in the differences in air temperature (ΔT), relative humidity (ΔRH), and humidity ratio (ΔW) for 23 ideal days in January and 15 ideal days in July over the three-year period.

5. Discussion

5.1. Generalizing the results

Variations in ΔRH_{X-D} exhibited a close inverse relationship with variations in ΔT_{X-D} throughout the year. Greater negative ΔRH_{X-D} values occurred during the nighttime when strong heat islands were present. The RH differences among the LCZ sites were significant during the nighttime but negligible during the daytime. For all LCZ sites, except for LCZ A (dense trees), no seasonal patterns in ΔRH_{X-D} were observed. Compared with LCZ D, LCZ A exhibited lower RH during the nighttime in winter but higher RH during the daytime in summer. RH during the nighttime were lower at LCZ G (water) than at LCZ D throughout the year. For all the urbanized LCZ sites, $\Delta RH_{X-D} < 0$ was clearly the dominant type both during the daytime and the nighttime.

For all LCZ sites, ΔW_{X-D} could be either positive (moisture excess) or negative (moisture deficit) throughout the year. Negative ΔW_{X-D} values

were more frequent and greater during the daytime and in the warm months, whereas positive ΔW_{X-D} occurred more frequently during the nighttime and in the cold months. The mean humidity ratio differences among the LCZ sites were not significant. No clear relationship was found between ΔW_{X-D} and ΔT_{X-D} . LCZ G exhibited more moisture than LCZ D ($\Delta W_{G-D} > 0$) during the nighttime but was drier ($\Delta W_{G-D} < 0$) during the daytime.

Inter-site humidity differences were better displayed under the ideal weather conditions (calm, clear). The frequency of urban moisture excess exhibited an increasing tendency during the nighttime with heavy condensation (dew and frost). Precipitation events significantly increased the frequency of urban moisture excess, and this effect could last until 24 h after precipitation. Humidity ratio differences were influenced by background meteorological parameters, but the trends were not clear. No relation was found between humidity ratio differences and heat island intensities.

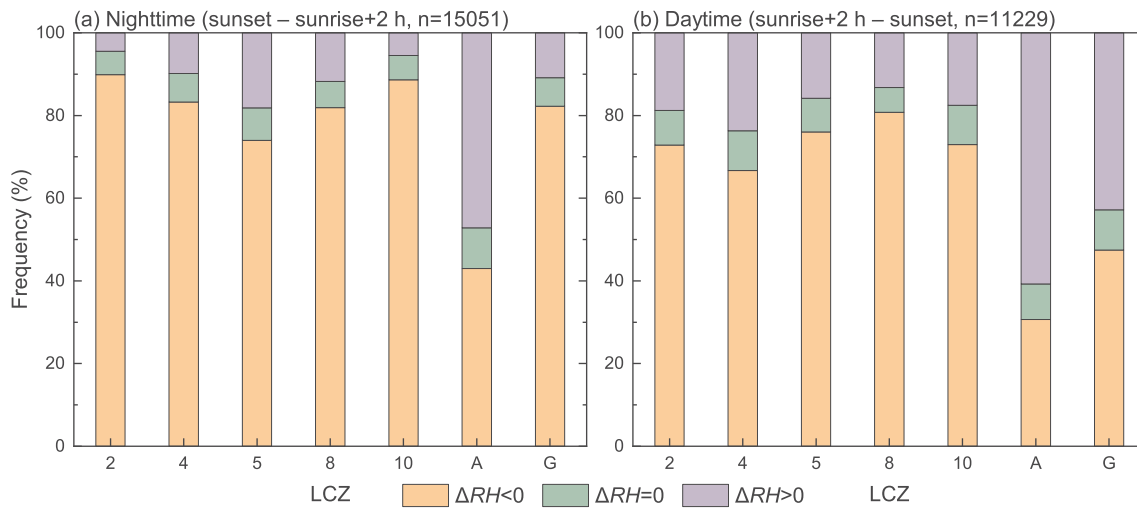


Fig. 9. Frequency of hourly ΔRH_{X-D} types for the three-year period: (a) nighttime; (b) daytime. ΔRH_{X-D} are the differences in relative humidity between the LCZ sites (LCZ X–LCZ D).

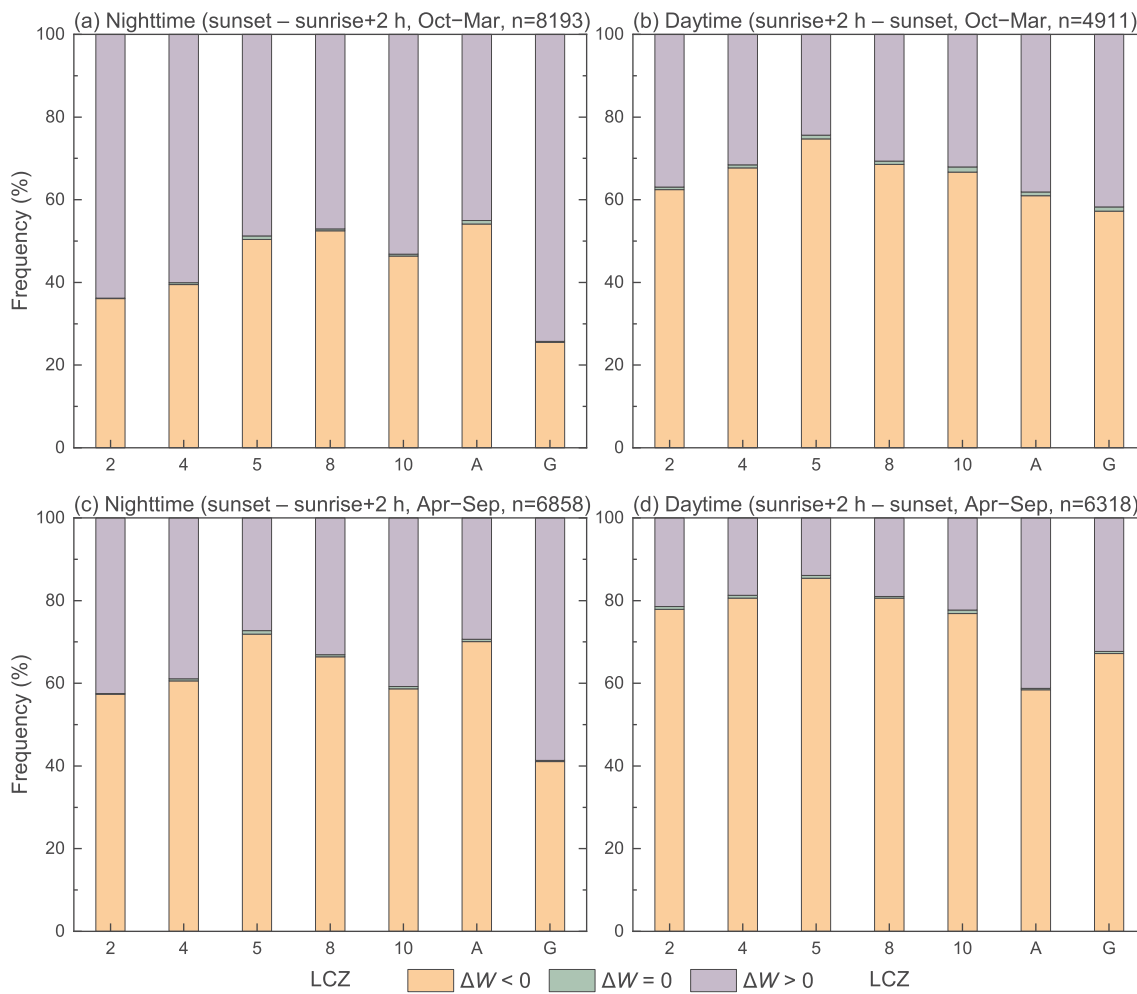


Fig. 10. Frequency of hourly ΔW_{X-D} types for the three-year period: (a) during the nighttime of October–March; (b) during the daytime of October–March; (c) during the nighttime of April–September; and (d) during the daytime of April–September. ΔW_{X-D} are the differences in humidity ratio between the LCZ sites (LCZ X–LCZ D).

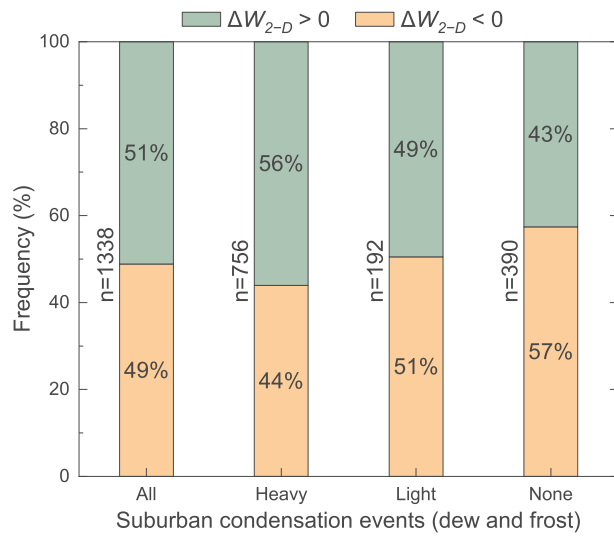


Fig. 11. Frequencies of hourly ΔW_{2-D} types on days with heavy, light, and none condensation events (dew and frost) during the 01:00 a.m.–06:00 a.m. period (All = 223 d; Heavy = 126 d; Light = 32 d; None = 65 d). ΔW_{2-D} are the differences in humidity ratio between LCZ 2 and LCZ D.

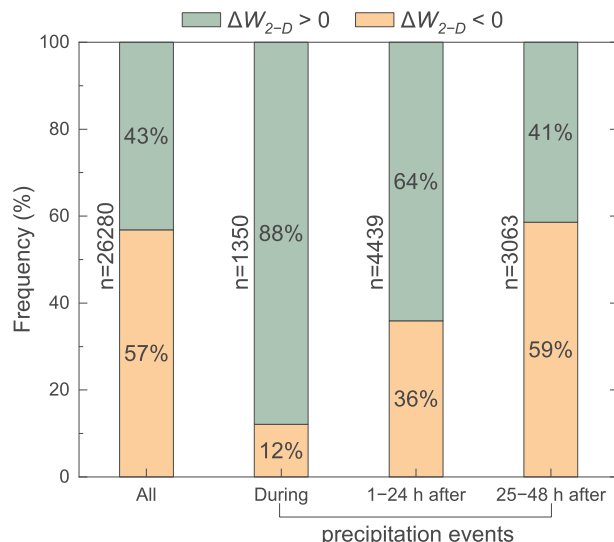


Fig. 12. Frequencies of hourly ΔW_{2-D} types for the whole three-year period (All), the period during precipitation events (During), the period within 24 h after precipitation events (1–24 h after), and the period within 25–48 h after precipitation events (25–48 h after). ΔW_{2-D} are the differences in humidity ratio between LCZ 2 and LCZ D.

5.2. Discussion on the results

The temporal pattern of ΔRH_{X-D} revealed in this study was generally consistent with the trend reported in previous studies (e.g. Refs. [13,17, 31,36]). The close relationship between ΔRH and ΔT demonstrates that relative humidity was largely controlled by temperature. $\Delta RH_{X-D} < 0$ occurred more frequently during the nighttime than during the daytime mainly because of the prevalence of nocturnal heat islands. The diurnal and seasonal patterns of water vapor differences between the urbanized LCZ sites and LCZ D were generally consistent with the findings from other cities, such as London [22], Shanghai [17], Beijing [34], and the Yangtze River Delta urban agglomeration [39]. However, a study in Edmonton [15] reported that the nocturnal vapor difference (urban–rural) was positive throughout the year and daytime vapor difference changed from a deficit in warm season to an excess in cold

season.

Notably, our results show that during the nighttime, RH values were lower at LCZ G than at LCZ D. This phenomenon is attributed to the nocturnal heat island caused by the large thermal inertia of water bodies. However, a previous study reported that a small lake tended to increase local relative humidity values [51]. Another notable feature is that LCZ G exhibited less moisture than LCZ D ($\Delta W_{G-D} < 0$) during the daytime. This finding differs from the common view that the surrounding area of water bodies is more humid than elsewhere. There may be several possible explanations for this. One possible explanation is that the lake (LCZ G) is located in the central area of the city (Fig. 1), surrounded by urban LCZ classes. The advection of dry air from the surrounding areas during the daytime might affect the measurements at LCZ G. Another possible explanation might be related to the lower daytime temperature gradient between water and the air above water than that at LCZ D, and consequently restraining the vertical turbulent transfer of water vapor at LCZ G. The experimental data of our earlier study [43] showed that the temperature gradient between the lake surface water and the air above water was smaller during the daytime but greater during the nighttime. During the daytime, the small temperature gradient over the lake weakens vertical turbulent transfer, leading to less water vapor being transferred into the air. Besides, during the daytime the relatively cool surface water temperature of the lake makes the overlying atmosphere to be stable. The water vapor pressure of the thin air layer near water tends to be saturated. Consequently, the small vapor pressure gradient between the water surface and overlying atmosphere will reduce evaporation. Further research is required to identify possible causes for the result of LCZ G.

Several studies indicated that the difference in dewfall between the urban and rural areas can affect the urban–rural humidity difference [15,30]. Specifically, rural dewfall tends to be higher than urban dewfall, and nocturnal urban moisture excess can be associated with reduced urban dew as less water vapor is removed from urban air [30]. Our results show an increasing tendency of urban moisture excess during the nighttime with heavy condensation, which supports the statement that compared with suburban or rural areas, less formation of dew and frost in urban area is contributing to nocturnal urban moisture excess.

Our results show that precipitation events significantly increased the frequency of urban moisture excess, and this effect could last until 24 h after the precipitation events. Numerous possible reasons for this can be identified. First, urban surface temperatures are commonly higher than rural areas, which results in more water being evaporated into urban atmosphere. Furthermore, the evaporated water vapor is more difficult to diffuse in urban canyons than at open, flat rural sites. Second, a large amount of heat stored by urban impervious fabric can continuously contribute to water evaporation during and after precipitation.

In this study, the comparison between all weather conditions and ideal weather conditions supports the claim that temporal patterns of urban–rural moisture differences are better displayed under ideal weather conditions [11]. The relationships between humidity ratio differences and cloud cover and solar irradiance indicate that the difference in evaporation rate between urban and rural sites is enlarged under clear weather conditions, causing greater and more frequent moisture deficits in urban areas. Our result shows that greater differences in humidity ratio occurred under relatively low wind speed conditions. This may be related to the fact that intense advection due to high wind speeds can reduce spatial differences in humidity.

Atmospheric water vapor can theoretically affect the longwave radiation balance. Thus, the urban–rural moisture difference may potentially play a role in UHI development. Hage [15] demonstrated that the urban–rural moisture difference does not play a crucial role in UHI development. Our results also show no clear relationship between humidity ratio differences and heat island intensities. However, some studies reported that urban moisture excess increases with an increase in UHI intensity [22,25,28,33]. Owing to the inconsistencies in previous studies and the current study, further investigations are needed.

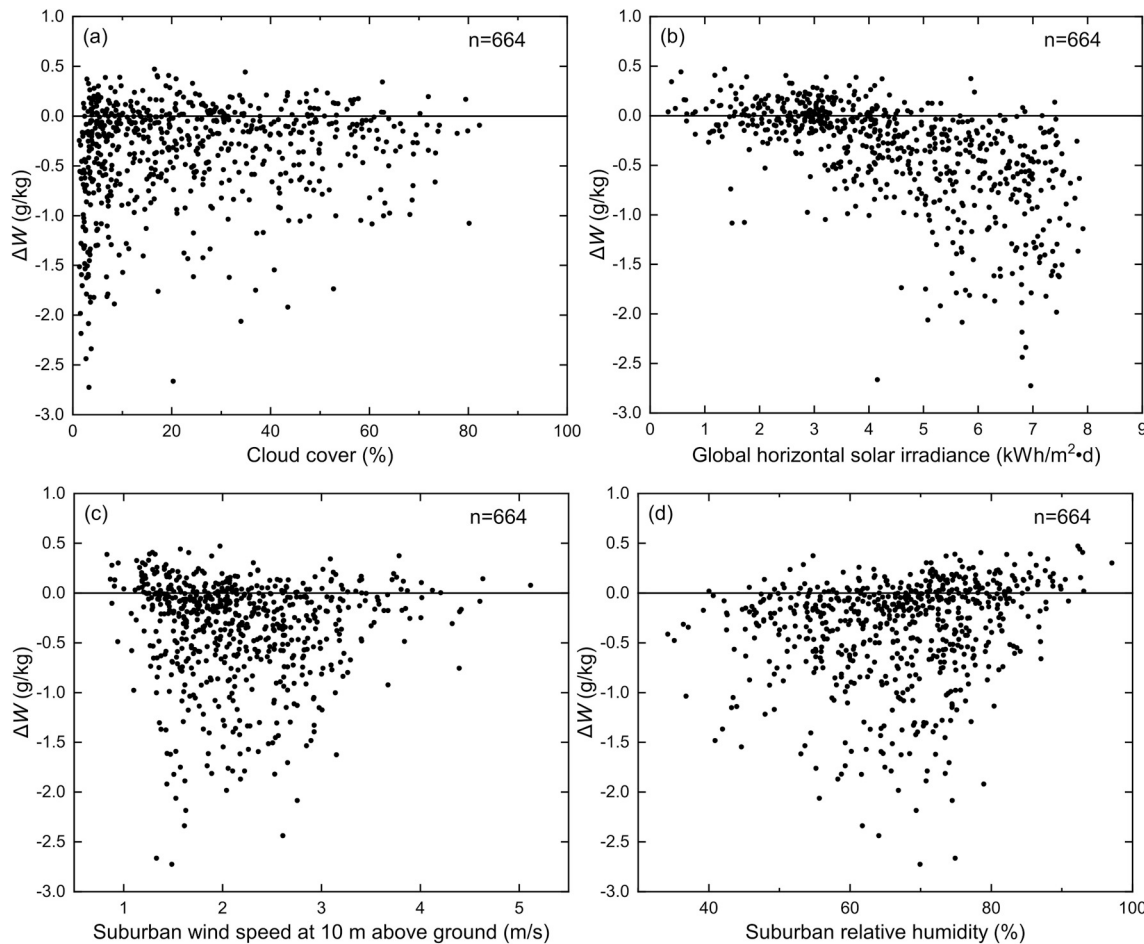


Fig. 13. Relationships between the daily average differences in humidity ratio (ΔW_{2-4}) and the daily averages of meteorological parameters: (a) cloud cover; (b) global horizontal solar irradiance; (c) suburban wind speed; and (d) suburban relative humidity. The days with precipitation have been excluded, leaving 664 days for analysis.

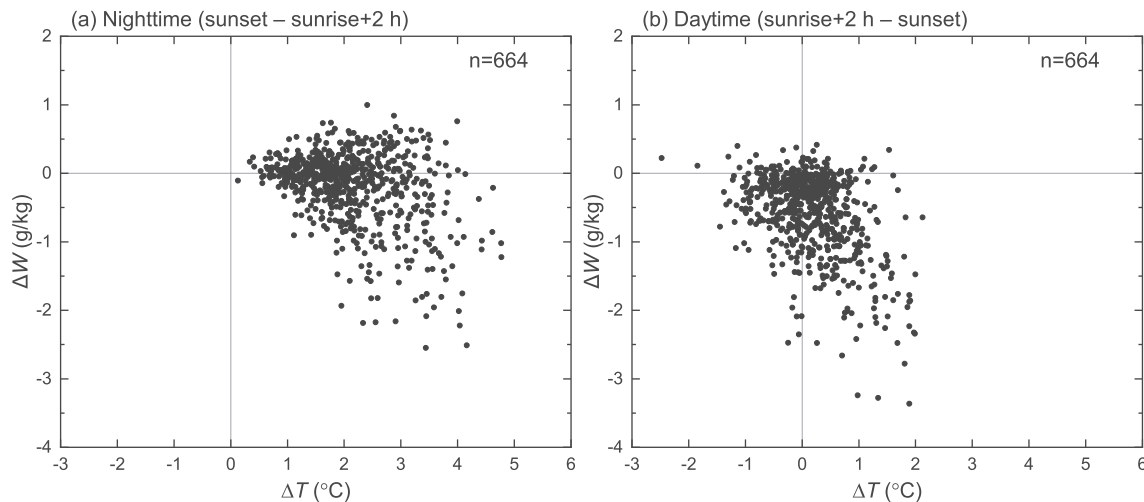


Fig. 14. Relationships between the daily differences in humidity ratio (ΔW_{2-4}) and the daily differences in temperature (ΔT_{2-4}): (a) nighttime averages; (b) daytime averages. The days with precipitation have been excluded, leaving 664 days for analysis.

It is necessary to point out that investigators from multiple fields can benefit from a robust understanding of the spatiotemporal characteristic of urban/rural humidity. For instance, some studies reported that relative humidity is associated with the presentations of diseases such as kidney stone [1], childhood hand, foot and mouth disease [2], and sickle

cell disease [3]. The study by Geletić et al. [8] showed that the LCZ scheme can be used for intra-urban comparison of thermal comfort. They also emphasized that humidity differences among LCZs is a non-negligible factor for thermal comfort assessment. The study by Jamriska et al. [5] showed that relative humidity could have a strong

influence on the concentration of traffic emission particles. Several studies indicated that neighborhood-scale humidity could affect the latent cooling load of buildings [52,53] and the condensation around air-conditioner's coils during summer [6]. Hence, humidity is an important factor for building cooling energy consumption, especially under hot and humid weather conditions. It is believed that the findings of this study will be valuable for different fields such as public health, outdoor thermal comfort, and building energy performance.

6. Conclusions

Atmospheric humidity in the urban canopy layer is an important aspect of urban physical environments. This study investigated the spatiotemporal characteristic of canopy-layer humidity differences of 8 local climate zones in Nanjing, China, on the basis of three-year hourly observations. Focus was directed toward the site-specific relative humidity and humidity ratio. The relationships of humidity ratio differences with condensation and precipitation events, meteorological parameters, and heat island intensities were also examined. The findings of this study can improve understanding of the spatiotemporal characteristic of urban/rural humidity at the local scale and will be valuable for multiple fields such as public health, outdoor thermal comfort, and building energy performance. In future studies, we suggest more attention should be paid to the comparison of observations from different cities, the possible physical mechanisms of urban/rural humidity features, and the relationships between urban design factors and urban humidity.

Declaration of competing interest

The authors declare that they have no known competing financial interests or personal relationships that could have appeared to influence the work reported in this paper.

Acknowledgements

This study was supported by the National Natural Science Foundation of China (grant numbers: 51408303, 41871189). The authors acknowledge the anonymous reviewers for their helpful and constructive comments.

References

- [1] M.E. Ross, A.M. Vicedo-Cabrera, R.E. Kopp, L. Song, D.S. Goldfarb, J. Pulido, S. Warner, S.L. Furth, G.E. Tasian, Assessment of the combination of temperature and relative humidity on kidney stone presentations, *Environ. Res.* 162 (2018) 97–105, <https://doi.org/10.1016/j.envres.2017.12.020>.
- [2] H. Yang, J. Wu, J. Cheng, X. Wang, L. Wen, K. Li, H. Su, Is high relative humidity associated with childhood hand, foot, and mouth disease in rural and urban areas? *Public Health* 142 (2017) 201–207, <https://doi.org/10.1016/j.puhe.2015.03.018>.
- [3] S. Jones, E.R. Duncan, N. Thomas, J. Walters, M.C. Dick, S.E. Height, A. D. Stephens, S.L. Thein, D.C. Rees, Windy weather and low humidity are associated with an increased number of hospital admissions for acute pain and sickle cell disease in an urban environment with a maritime temperate climate, *Br. J. Haematol.* 131 (2005) 530–533, <https://doi.org/10.1111/j.1365-2141.2005.05799.x>.
- [4] H.K. Elminir, Dependence of urban air pollutants on meteorology, *Sci. Total Environ.* 350 (2005) 225–237, <https://doi.org/10.1016/j.scitotenv.2005.01.043>.
- [5] M. Jamriska, L. Morawska, K. Mergersen, The effect of temperature and humidity on size segregated traffic exhaust particle emissions, *Atmos. Environ.* 42 (2008) 2369–2382, <https://doi.org/10.1016/j.atmosenv.2007.12.038>.
- [6] T. Ihara, Y. Genchi, T. Sato, K. Yamaguchi, Y. Endo, City-block-scale sensitivity of electricity consumption to air temperature and air humidity in business districts of Tokyo, Japan, *Energy* 33 (2008) 1634–1645, <https://doi.org/10.1016/j.energy.2008.06.005>.
- [7] X. Wang, Y. Gong, The impact of an urban dry island on the summer heat wave and sultry weather in Beijing City, *Chin. Sci. Bull.* 55 (2010) 1657–1661, <https://doi.org/10.1007/s11434-010-3088-5>.
- [8] J. Geletić, M. Lehnert, S. Savić, D. Milošević, Modelled spatiotemporal variability of outdoor thermal comfort in local climate zones of the city of Brno, Czech Republic, *Sci. Total Environ.* 624 (2018) 385–395, <https://doi.org/10.1016/j.scitotenv.2017.12.076>.
- [9] L. Julia, T.H. Sparks, E. Nicole, M. Annette, Does humidity trigger tree phenology? Proposal for an air humidity based framework for bud development in spring, *New Phytol.* 202 (2014) 350–355, <https://doi.org/10.1111/nph.12680>.
- [10] H. Gupta, C. Tiwari, S. Diwakar, Butterfly diversity and effect of temperature and humidity gradients on butterfly assemblages in a sub-tropical urban landscape, *Trop. Ecol.* 60 (2019) 150–158, <https://doi.org/10.1007/s42965-019-00019-y>.
- [11] T.R. Oke, G. Mills, A. Christen, J.A. Voogt, *Urban Climates*, Cambridge University Press, 2017, pp. 254–268.
- [12] I.D. Stewart, T.R. Oke, Local climate zones for urban temperature studies, *Bull. Am. Meteorol. Soc.* 93 (2012) 1879–1900, <https://doi.org/10.1175/BAMS-D-11-00019.1>.
- [13] T.J. Chandler, Absolute and relative humidities in towns, *Bull. Am. Meteorol. Soc.* 48 (1967) 394–399, <https://doi.org/10.1175/1520-0477-48.6.394>.
- [14] R.J. Kopec, Daily spatial and secular variations of atmospheric humidity in a small city, *J. Appl. Meteorol.* 12 (1973) 639–648, [https://doi.org/10.1175/1520-0450\(1973\)012<0639:DSASVO>2.0.CO;2](https://doi.org/10.1175/1520-0450(1973)012<0639:DSASVO>2.0.CO;2).
- [15] K.D. Hage, Urban-rural humidity differences, *J. Appl. Meteorol.* 14 (1975) 1277–1283, [https://doi.org/10.1175/1520-0450\(1975\)014<1277:URHD>2.0.CO;2](https://doi.org/10.1175/1520-0450(1975)014<1277:URHD>2.0.CO;2).
- [16] D.L. Sisterson, R.A. Dirks, Structure of the daytime urban moisture field, *Atmos. Environ.* 12 (1978) 1943–1949, [https://doi.org/10.1016/0004-6981\(78\)90129-4](https://doi.org/10.1016/0004-6981(78)90129-4).
- [17] D.C. Shu, C. Chao, Shanghai urban influences on humidity and precipitation distribution, *Geojournal* 8 (1984) 201–204, <https://doi.org/10.1007/BF00446468>.
- [18] J.A. Henry, S.E. Dicks, G.A. Marotz, Urban and rural humidity distributions: relationships to surface materials and land use, *J. Climatol.* 5 (1985) 53–62, <https://doi.org/10.1002/joc.3370050105>.
- [19] S.W. Brazel, R.C. Balling, Temporal analysis of long term atmospheric moisture levels in Phoenix, Arizona, *J. Clim. Appl. Meteorol.* 25 (1986) 112–117, [https://doi.org/10.1175/1520-0450\(1986\)025<0112:TAOLTA>2.0.CO;2](https://doi.org/10.1175/1520-0450(1986)025<0112:TAOLTA>2.0.CO;2).
- [20] B. Ackerman, Climatology of Chicago area urban-rural differences in humidity, *J. Clim. Appl. Meteorol.* 26 (1987) 427–430, [https://doi.org/10.1175/1520-0450\(1987\)026<0427:COCAUR>2.0.CO;2](https://doi.org/10.1175/1520-0450(1987)026<0427:COCAUR>2.0.CO;2).
- [21] Y.R. Adebayo, The effect of urbanization on some characteristics of relative humidity in Ibadan, *J. Climatol.* 7 (1987) 599–607, <https://doi.org/10.1002/joc.3370070608>.
- [22] D.O. Lee, Urban-rural humidity differences in London, *Int. J. Climatol.* 11 (1991) 577–582, <https://doi.org/10.1002/joc.3370110509>.
- [23] Y.R. Adebayo, Day-time effects of urbanization on relative humidity and vapour pressure in a tropical city, *Theor. Appl. Climatol.* 43 (1991) 17–30, <https://doi.org/10.1007/BF00865039>.
- [24] E. Jáuregui, A. Tejeda, Urban-rural humidity contrasts in Mexico City, *Int. J. Climatol.* 17 (1997) 187–196, [https://doi.org/10.1002/\(SICI\)1097-0088\(199702\)17:2<187:AID-JOC114>3.0.CO;2-P](https://doi.org/10.1002/(SICI)1097-0088(199702)17:2<187:AID-JOC114>3.0.CO;2-P).
- [25] B. Holmer, I. Eliasson, Urban-rural vapour pressure differences and their role in the development of urban heat islands, *Int. J. Climatol.* 19 (1999) 989–1009, [https://doi.org/10.1002/\(SICI\)1097-0088\(199907\)19:9<989:AID-JOC410>3.0.CO;2-1](https://doi.org/10.1002/(SICI)1097-0088(199907)19:9<989:AID-JOC410>3.0.CO;2-1).
- [26] J. Unger, Urban-rural air humidity differences in Szeged, Hungary, *Int. J. Climatol.* 19 (1999) 1509–1515, [https://doi.org/10.1002/\(SICI\)1097-0088\(19991115\)19:13<1509:AID-JOC453>3.0.CO;2-P](https://doi.org/10.1002/(SICI)1097-0088(19991115)19:13<1509:AID-JOC453>3.0.CO;2-P).
- [27] V. Deosthal, Impact of rapid urban growth on heat and moisture islands in Pune City, India, *Atmos. Environ.* 34 (2000) 2745–2754, [https://doi.org/10.1016/S1352-2310\(99\)00370-2](https://doi.org/10.1016/S1352-2310(99)00370-2).
- [28] M. Unkăsević, O. Jovanović, T. Popović, Urban-suburban/rural vapour pressure and relative humidity differences at fixed hours over the area of Belgrade city, *Theor. Appl. Climatol.* 68 (2001) 67–73, <https://doi.org/10.1007/s007040170054>.
- [29] H. Mayer, A. Matzarakis, M.G. Izquierdo, Spatio-temporal variability of moisture conditions within the urban canopy layer, *Theor. Appl. Climatol.* 76 (2003) 165–179, <https://doi.org/10.1007/s00704-003-0010-y>.
- [30] K. Richards, Urban and rural dewfall, surface moisture, and associated canopy-level air temperature and humidity measurements for Vancouver, Canada, *Boundary-Land Meteorol.* 114 (2005) 143–163, <https://doi.org/10.1007/s10546-004-8947-7>.
- [31] K. Fortuniak, K. Klysik, J. Wibig, Urban-rural contrasts of meteorological parameters in Łódź, *Theor. Appl. Climatol.* 84 (2006) 91–101, <https://doi.org/10.1007/s00704-005-0147-y>.
- [32] H. Um, K. Ha, S. Lee, Evaluation of the urban effect of long-term relative humidity and the separation of temperature and water vapor effects, *Int. J. Climatol.* 27 (2007) 1531–1542, <https://doi.org/10.1002/joc.1483>.
- [33] W. Kuttler, S. Weber, J. Schonefeld, A. Hesselschwerdt, Urban/rural atmospheric water vapour pressure differences and urban moisture excess in Krefeld, Germany, *Int. J. Climatol.* 27 (2007) 2005–2015, <https://doi.org/10.1002/joc.1558>.
- [34] W. Liu, H. You, J. Dou, Urban-rural humidity and temperature differences in the Beijing area, *Theor. Appl. Climatol.* 96 (2009) 201–207, <https://doi.org/10.1007/s00704-008-0024-6>.
- [35] B. Holmer, S. Thorsson, J. Lindén, Evening evapotranspirative cooling in relation to vegetation and urban geometry in the city of Ouagadougou, Burkina Faso, *Int. J. Climatol.* 33 (2013) 3089–3105, <https://doi.org/10.1002/joc.3561>.
- [36] D. Vujošić, N. Todorović, Urban-rural fog differences in Belgrade area, Serbia, *Theor. Appl. Climatol.* 131 (2018) 889–898, <https://doi.org/10.1007/s00704-016-2019-z>.
- [37] E. Masiero, L.C.L.D. Souza, Mapping humidity plume over local climate zones in a high-altitude tropical climate city, Brazil, *Ambiente Construído* 18 (2018) 177–197, <https://doi.org/10.1590/s1678-86212018000400300>.
- [38] J. Zhang, L. Wu, The influence of population movements on the urban relative humidity of Beijing during the Chinese Spring Festival holiday, *J. Clean. Prod.* 170 (2018) 1508–1513, <https://doi.org/10.1016/j.jclepro.2017.09.274>.

- [39] M. Luo, N.C. Lau, Urban expansion and drying climate in an urban agglomeration of east China, *Geophys. Res. Lett.* 46 (2019) 6868–6877, <https://doi.org/10.1029/2019GL082736>.
- [40] M.C. Peel, B.L. Finlayson, T.A. McMahon, Updated world map of the Köppen-Geiger climate classification, *Hydrol. Earth Syst. Sci.* 11 (2007) 259–263.
- [41] M. Palme, L. Inostroza, G. Villacreses, A. Lobato-Cordero, C. Carrasco, From urban climate to energy consumption. Enhancing building performance simulation by including the urban heat island effect, *Energy Build.* 145 (2017) 107–120, <https://doi.org/10.1016/j.enbuild.2017.03.069>.
- [42] China Meteorological Bureau, Tsinghua University, *China Standard Weather Data for Analyzing Building Thermal Conditions*, China Building Industry Publishing House, 2005 ([in Chinese]).
- [43] X. Yang, L. Yao, T. Jin, L.L.H. Peng, Z. Jiang, Z. Hu, Y. Ye, Assessing the thermal behavior of different local climate zones in the Nanjing metropolis, China, *Build. Environ.* 137 (2018) 171–184, <https://doi.org/10.1016/j.buildenv.2018.04.009>.
- [44] I.D. Stewart, T.R. Oke, E.S. Krayenhoff, Evaluation of the 'local climate zone' scheme using temperature observations and model simulations, *Int. J. Climatol.* 34 (2014) 1062–1080, <https://doi.org/10.1002/joc.3746>.
- [45] F. Leconte, J. Bouyer, R. Claverie, M. Pétrissans, Using Local Climate Zone scheme for UHI assessment: evaluation of the method using mobile measurements, *Build. Environ.* 83 (2015) 39–49, <https://doi.org/10.1016/j.buildenv.2014.05.005>.
- [46] N. Skarbit, I.D. Stewart, J. Unger, T. Gál, Employing an urban meteorological network to monitor air temperature conditions in the 'local climate zones' of Szeged, Hungary, *Int. J. Climatol.* 37 (2017) 582–596, <https://doi.org/10.1002/joc.5023>.
- [47] R. Kotharkar, A. Bagade, Evaluating urban heat island in the critical local climate zones of an Indian city, *Lands. Urban Plan.* 169 (2018) 92–104, <https://doi.org/10.1016/j.landurbplan.2017.08.009>.
- [48] U.S. Department of Energy, EnergyPlus, version 8.9.0, <https://energyplus.net/>, accessed 2 June 2018.
- [49] T.R. Oke, An Algorithmic Scheme to Estimate Hourly Heat Island Magnitude, 2nd Urban Environment Symposium, Albuquerque, NM, November 1998, pp. 2–6.
- [50] T.R. Oke, Boundary Layer Climates, second ed., Routledge, London and New York, 1987, pp. 373–374, hardback version 2015.
- [51] H. Saaroni, B. Ziv, The impact of a small lake on heat stress in a Mediterranean urban park: the case of Tel Aviv, Israel, *Int. J. Biometeorol.* 47 (2003) 156–165, <https://doi.org/10.1007/s00484-003-0161-7>.
- [52] X. Yang, L. Zhao, M. Bruse, Q. Meng, An integrated simulation method for building energy performance assessment in urban environments, *Energy Build.* 54 (2012) 243–251, <https://doi.org/10.1016/j.enbuild.2012.07.042>.
- [53] J. Bouyer, C. Inard, M. Musy, Microclimatic coupling as a solution to improve building energy simulation in an urban context, *Energy Build.* 43 (2011) 1549–1559, <https://doi.org/10.1016/j.enbuild.2011.02.010>.